Geology

Plant-driven fungal weathering: Early stages of mineral alteration at the nanometer scale

Steeve Bonneville, Mark M. Smits, Andrew Brown, John Harrington, Jonathan R. Leake, Rik Brydson and Liane G. Benning

Geology 2009;37;615-618
doi:10.1130/G25699A.1

Notes

Plant-driven fungal weathering: Early stages of mineral alteration at the nanometer scale

Steeve Bonneville[1*], Mark M. Smits[2], Andrew Brown[3], John Harrington[3], Jonathan R. Leake[2], Rik Brydson[3], and Liane G. Benning[1]

[1]Earth and Biosphere Institute, School of Earth and Environment, University of Leeds, Leeds LS2 9JT, UK

[2]Department of Animal and Plant Sciences, University of Sheffield, Western Bank, Sheffield S10 2TN, UK

[3]Leeds Electron Microscopy and Spectroscopy Centre, Institute for Materials Research, University of Leeds, Leeds LS2 9JT, UK

ABSTRACT

Plant-driven fungal weathering is a major pathway of soil formation, yet the precise mechanism by which mycorrhiza alter minerals is poorly understood. Here we report the first direct in situ observations of the effects of a soil fungus on the surface of a mineral over which it grew in a controlled experiment. An ectomycorrhizal fungus was grown in symbiosis with a tree seedling so that individual hyphae expanded across the surface of a biotite flake over a period of three months. Ultramicroscopic and spectroscopic analysis of the fungus-biotite interfaces revealed intimate fungal-mineral attachment, biomechanical forcing, altered interlayer spacings, substantial depletion of potassium (~50 nm depth), oxidation of the biotite Fe(II), and the formation of vermiculite and clusters of Fe(III) oxides. Our study demonstrates the biomechanical-chemical alteration interplay at the fungus-biotite interface at the nanometer scale. Specifically, the weathering process is initiated by physical distortion of the lattice structure of biotite within 1 μm of the attached fungal hypha. Only subsequently does the distorted volume become chemically altered through dissolution and oxidation reactions that lead to mineral neoformation.

INTRODUCTION

Many rocks at the Earth's surface were formed originally at high temperature and pressure in a reducing environment. Tectonic forces have now exposed them to the slow but inevitable action of oxygenated solutions that trigger chemical reactions and physical alterations, resulting in the formation of secondary mineral phases, such as clays, that are more stable at Earth's surface conditions. Resistant primary and secondary minerals are redistributed to form sediments and soils upon which the entire terrestrial biosphere depends. Rock weathering through dissolution reactions also affects the chemical compositions of ground water, river and lake water, and ultimately oceans (Banfield and Nealson, 1997). Therefore, weathering leads to a major geochemical fractionation near the Earth's surface. Over geological time, such processes have contributed to shape the compositions of the mantle, crust, hydrosphere, and atmosphere (Berner, 2004).

While rock weathering was classically thought of as an inorganic process, it is now recognized that plants, and especially forests, accelerate weathering rates by a factor of 4 to 10 compared to geologically similar, nonvegetated areas (Moulton et al., 2000). More than 80% of plant roots form symbiotic associations (mycorrhiza) with soil fungi, and in boreal and temperate regions, as much as 90% of the woody tree root tips are covered by ectomycorrhizal fungal sheaths (as much as 600 km of fungal mycelium per kg of soil) (Ek, 1997; Read and Perez-Moreno, 2003). Thus, virtually all nutrients taken up by trees pass through these fungi, and in return, the fungi receive 20%–30% of the carbon fixed during photosynthesis by the host plants (Högberg and Högberg, 2002). Therefore, the fungi play a key role in the mineralogical modification that characterizes weathering, removing, for example, K, P, Ca, Mg, and Fe, and providing carbon that becomes fixed into soil carbonate minerals (Balogh-Brunstad et al., 2008). This link between biological mineral weathering and photosynthesis may have played a crucial role in the Earth's climate history (Beerling and Berner, 2005). Kennedy et al. (2006) suggested that the expansion of soil biota and especially fungi during the Late Proterozoic helped create conditions suitable for animal life. Indeed, molecular clock evidence suggests that fungi appeared on land ca. 700 Ma ago (Heckman et al., 2001) and the earliest fossil record of mycorrhiza dates from 400 Ma ago (Remy et al., 1994). The acceleration of weathering kinetics due to the action of soil fungi increased the formation of clay minerals, which efficiently bind organic matter, and hence this process favored carbon burial in soils and in continental margins. This increased carbon sequestration coupled to photosynthesis may have triggered the rise in atmospheric oxygen levels in the Late Proterozoic that allowed the development of large terrestrial eukaryotic organisms (Derry, 2006).

Hitherto, mineral weathering by mycorrhizal fungi was postulated to rely primarily on the ability of fungi to exude organic ligands and protons and thus alter soil solution composition (Adeyemi and Gadd, 2005; Gadd, 2007; Kraemer, 2004; Wallander and Wickman, 1999). However, most mycorrhizal fungi grow in unsaturated soils and are intolerant of waterlogging. Their mycelial networks strongly attach to mineral surfaces, and therefore weathering processes are likely to be initiated and to proceed directly at the mineral-fungi interface. This interface therefore, may play a far greater role in initiating and controlling the weathering rates than previously thought. We report here, for the first time, in situ observations at the nanometer scale of the early stages of weathering of biotite by an ectomycorrhizal fungus, *Paxillus involutus*, grown under axenic and controlled temperature, humidity, and photoperiod conditions in symbiosis with a boreal pine tree, *Pinus sylvestris* (Fig. 1A; see also the GSA Data Repository[1]). This approach recreates the essential symbiotic relationship between the tree and the mycorrhizal fungus under the typical unsaturated conditions found in soils, while excluding all other potential weathering pathways (i.e., soil pore water and other soil microorganisms).

METHODS

Pinus sylvestris (Scots pine) and *Paxillus involutus* (ectomycorrhizal fungi) were first grown separately on cellophane-covered agar plates under aseptic conditions for four weeks. Seedlings of *Pinus sylvestris* were then aseptically transferred onto *Paxillus involutus* cultivated plates. After 10 weeks of growth, roots of *Pinus sylvestris* were well colonized and had developed a symbiotic relationship with the fungi, *Paxillus involutus*, as evidenced by the formation of characteristic short "T" shape roots entangled in dense hyphal networks. Both tree and fungi were then trans-

*E-mail: s.bonneville@see.leeds.ac.uk.

[1]GSA Data Repository item 2009144, (1) methods for cultivation, ion milling, TEM analysis and chemical composition of biotite and growth medium; (2) observations of hypha by Environmental SEM at various hydration states; and (3) raw data of STEM-EDS of lamella 3, is available online at www.geosociety.org/pubs/ft2009.htm, or on request from editing@geosociety.org or Documents Secretary, GSA, P.O. Box 9140, Boulder, CO 80301, USA.

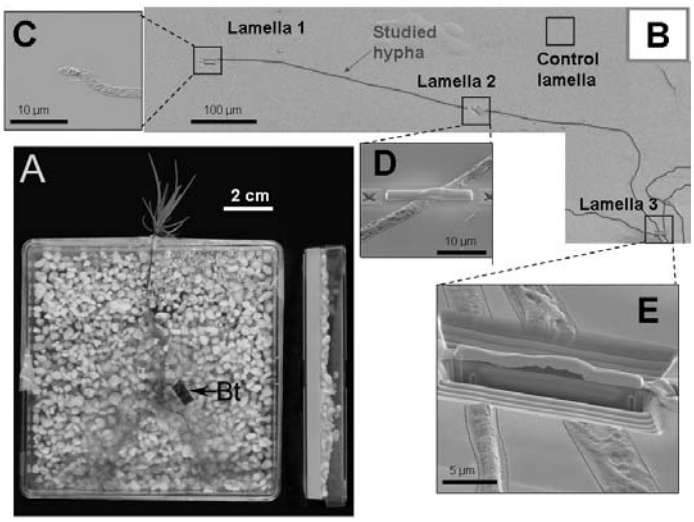

Figure 1. A: Experimental microcosm. Bt—biotite. B: Photomicrograph of positions of three lamellae along a single hypha and control lamella that represent a sequence of hypha-biotite contact period with lamella 3 > lamella 2 > lamella 1. C: Photomicrograph of hypha tip before milling of lamella 1. D: Deposition of platinum strap prior to cutting of lamella 2. E: Ion milled trench across lamella 3 (details in Methods and Fig. DR1; see footnote 1).

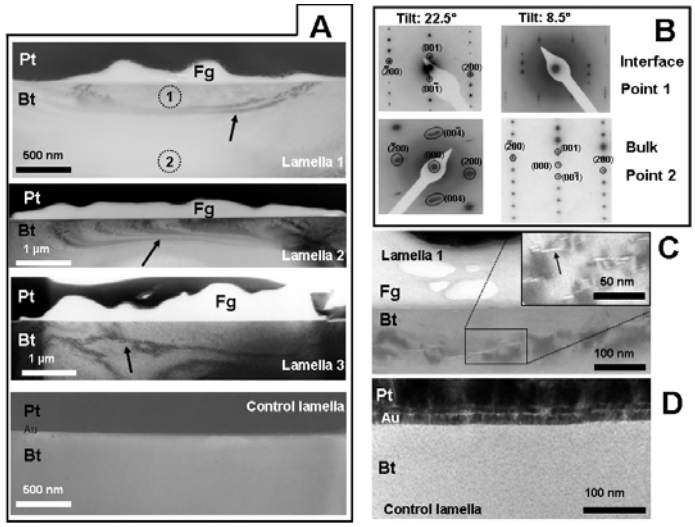

Figure 2. A: Bright-field transmission electron microscope micrographs of hypha-biotite lamellae 1–3 showing curvilinear diffraction contrast in the biotite in contrast to the control lamella (bottom). B: Selected area electron diffraction patterns of the interfacial versus bulk biotite in lamella 1 (index on biotite monoclinic structure; JCPDS reference 01–074–2578). The biotite crystal structure was tilted from a relative angle of 8.5° in the bulk (point 2) to an angle of 22.5° at the interface with the hypha tip (point 1) to obtain the same [0$\bar{1}$0] zone axis diffraction patterns (zone axis parallel to the electron beam). C: Microcavities in lamella 1. D: Detailled view of control lamella. Pt—platinum coating, Fg—fungal hypha, Bt—biotite, Au—gold coating.

ferred together to a microcosm setup in which a freshly cleaved biotite flake (~0.5 × 1 cm) was placed as the main source of potassium in the system (Fig. 1A; for details on media and biotite chemical composition, see the Data Repository). The microcosm system was incubated for 19 weeks in a climate-controlled room at 15 ºC day and 10 ºC night temperature, with an 18 h photoperiod (550 µmol m^{-2} s^{-1} irradiance), and with the shoots exposed to 80% humidity. After fungal-mineral contact of as much as three months, the biotite was retrieved and three lamellae were cut from the biotite immediately beneath a single strand of fungal hypha using a focused ion beam (FIB). An additional lamella was cut from an adjacent hyphae-free area of the biotite surface as a control (Figs. 1B–1E and DR1; see the Data Repository). The lamellae were imaged and analyzed using transmission electron microscopy (TEM) and scanning transmission X-ray microscopy (STXM) (see the Data Repository for details).

RESULTS

Bright-field TEM images of the three hypha-biotite lamellae exhibit strong diffraction contrasts at the interface, evidenced by a curved dark and/or black halo across a region in close vicinity with the hypha (Fig. 2A). These diffraction contrasts arise from differences in biotite crystal lattice orientation across each lamella. For example, in the youngest section (i.e., shortest hypha-biotite contact time; lamella 1, Fig. 2B), selected area electron diffraction (SAED) patterns of the biotite close to the interface (~top 200 nm below interface; point 1 in Fig. 2A) and the bulk biotite (~1 µm below interface; point 2 in Fig. 2A) confirmed that the biotite crystal structure close to the interface was misoriented by an angle of at least 14° relative to the bulk, the biotite crystal at the interface being oriented parallel to the [0$\bar{1}$0] zone axis. Such diffraction contrast was not observed in the control lamella (Fig. 2A), suggesting that the biotite lattice distortion was related to the presence of the hypha. Tilting the FIB lamellae with respect to the incident TEM beam revealed that the contrast originated from a region ~300 nm, ~500 nm, and ~1 µm below the biotite interface for lamellae 1, 2, and 3, respectively. Further indications of the mechanical stress applied to the biotite were cleavage-parallel microcavities observed in the biotite close to the interface with the hypha; such features were not observed in the control lamella (Figs. 2C and 2D). Strain artifacts due to hyphal dehydration and shrinkage during exposure to the microscope vacuum were discounted (see Fig. DR2 and the Data Repository text).

Atomic lattice-resolution TEM imaging of the three lamellae shows an intimate contact between the fungus and biotite surfaces (Fig. 3). Biotite exhibits the characteristic mica structure consisting of alternating tetrahedrally and octahedrally coordinated sheets (T-O-T layers) stacked along the [001] direction with interlayer planes of potassium ions. At the hypha-biotite interface in lamella 1, despite the lattice distortion extending to ~300 nm, phase-contrast TEM imaging showed lattice planes parallel to the biotite surface with 1.0 nm spacing, consistent with the typical [001] biotite spacing (Fig. 3A). With continuing exposure to the hyphae, in lamella 2, the biotite [001] planes were still mostly intact (interlayer spacing still ~1.0 nm; Fig. 3B), yet slight bending of the [001] planes was visible, together with a disruption of the top 2–3 interfacial layers, indicating the initiation of mineral dissolution (black arrow in Fig. 3B). The lattice images corresponding to the longest contact between hyphae and biotite (lamella 3) revealed numerous dislocations or stacking faults in the layered biotite structure (white arrows in Fig. 3C), indicating substantial structural disruption. Furthermore, secondary mineral formation in the zone close to the hyphae-biotite interface was observed: in some regions, the [001] plane spacings were expanded from 1.0 nm to 1.4 nm and even 3.0 nm (arrows in Figs. 3C and 3D), suggestive of vermiculite formation (Wierzchos and Ascaso, 1998). Finally, a few poorly defined regions exhibited lattice spacings of ~0.32 nm associated with disruption of the [001] biotite planes (inset Fig. 3D), likely indicating the presence of ferrihydrite.

The presence of Fe(III) oxide clusters close to the hypha-biotite interface in lamella 3 implies partial oxidation of the Fe(II) in the biotite lattice. Spatially resolved X-ray absorption near edge structure (XANES) spectra recorded using STXM of lamella 2 confirmed that a large proportion of the iron was present as ferric iron (+III oxidation state) in the top

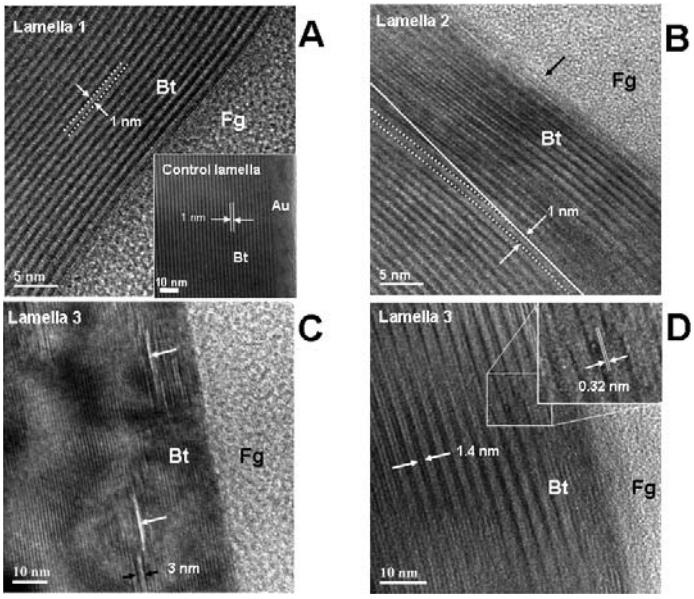

Figure 3. Atomic lattice-resolution transmission electron microscope micrographs of biotite-hypha interface. A: Lamella 1. B: Lamella 2. C, D: Lamella 3. Fg—fungal hypha, Bt—biotite, Au—gold coating.

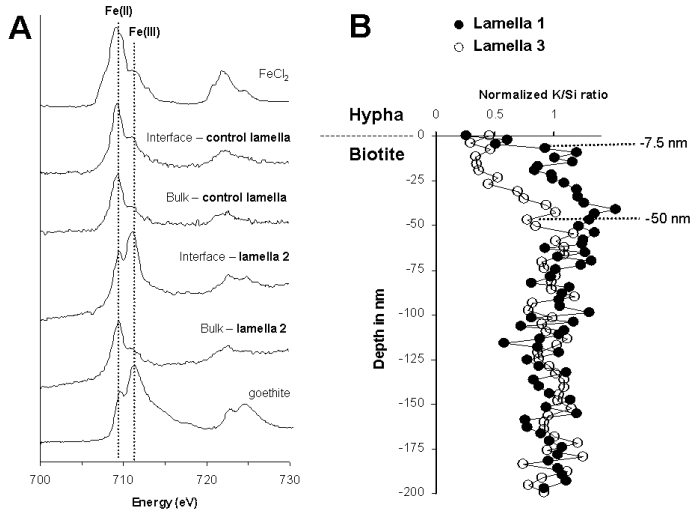

Figure 4. A: Fe $L_{2,3}$ edge X-ray absorption near edge structure spectra of both interfacial and bulk biotite in lamella 2 and control lamella. $FeCl_2$ (top spectrum) and FeOOH (goethite; bottom spectra) were used as reference materials for the Fe L_3 peak positions for Fe(II) and Fe(III) at 709.3 and 711.3 eV, respectively. B: Comparison of K/Si elemental ratios across interface determined by scanning transmission electron microscope–energy dispersive X-ray (STEM-EDX) showing potassium depletion zone in the biotite for lamella 1 (full circles) and lamella 3 (open circles). The K/Si elemental ratios have been normalized to average bulk K/Si biotite ratios in each lamella (Table DR1; see footnote 1).

100 nm at the biotite interface, while ~2 μm away from the interface all Fe was still in its ferrous form (+II), as expected for unaltered biotite. Scanning TEM-energy dispersive X-ray (STEM-EDX) elemental profiles across the interface of lamella 3 with the hypha showed significant potassium depletion close to the interface when compared to lamella 1 (Figs. 4B and DR3). In lamella 3, within 50 nm of the hypha-biotite interface, the normalized K/Si ratio drops from an average value of 1 to 0.3–0.5 corresponding to ~50%–70% potassium depletion, while in lamella 1, potassium depletion was limited to the top 5–10 nm. Because the STEM beam size was 5 nm in diameter, we interpreted the potassium depletion at the interface in lamella 1 to be minimal and the observed depletion to be a convolution effect (i.e., measurement artifact due to the beam spot size resulting in a broadening of the interface). Probably at the hypha tip, the contact period was too short to induce significant potassium depletion.

DISCUSSION

Within our sequence of lamella, the biotite in lamella 1 underwent only a mechanical shear of the lattice structure, extending to 300 nm in depth (Fig. 2A). As the biotite-hypha exposure time increased (lamella 2 and 3), in addition to mechanical shear, chemical alteration is evidenced by Fe(II) oxidation (Fig. 4A), significant potassium depletion (Fig. 4B), and the formation of vermiculite and ferrihydrite (Figs. 3C and 3D). The lattice distortion at the hyphae-biotite contact is likely a consequence of fungal attachment and growth across the biotite surface. Fungal attachment to mineral surfaces usually occurs via class I hydrophobins, which are ubiquitous hyphal surface proteins of basidiomycete fungi (Wosten et al., 1993) such as *P. involutus*, and which allow the hypha to bind strongly to virtually all mineral surfaces. In addition to their adhesion abilities, within hyphal tips, the internal hyphal pressures can vary between 0.4 and 1 MPa (Harold, 2002) (one or two orders of magnitudes higher than other soil microorganisms can achieve) and reach as high as 8 MPa (or 80 bars) in specialized penetrative structures (appressoria) (Bechinger et al., 1999). This high internal pressure is believed to both drive the hyphal growth (Bastmeyer et al., 2002) and be an evolutionary adaptation to penetrate plant tissue and rock surfaces (Jongmans et al., 1997; Money, 1999). Abiotic biotite deformation experiments have generated structural dislocations at relatively low shear stresses (i.e., 0.1 as much as 3 MPa for both [001] and [010] directions; Noe et al., 1999), well within the range of known hyphae pressures. In addition, in lamella 1, the mechanical stress in the biotite close to the interface occurs without changes in the diffraction patterns (i.e., SAED patterns from point 1 and 2 in Fig. 2B were indexed using the same biotite data set; Joint Committee on Powder Diffraction Standards [JCPDS] reference 01–074–2578), yet the orientation of the biotite crystal structure changed. Therefore, hydration processes at the interface that would have affected the diffraction pattern (i.e., change in interplanar distances measured by SAED) were ruled out. In addition, no obvious chemical changes were observed in the STEM-EDS analysis of lamella 1 (Fig. 4B). All these lines of evidence suggest that the high internal pressure of the hypha tip, especially during growth, combined with the firm adhesion of the growing hyphae to the biotite surface, may create a downward component of force and/or stress large enough to mechanically affect the biotite crystal structure orientation.

The increase in size of the potassium depletion zone between lamellae 1 and 3 suggests a progressive potassium transfer from the biotite to the hypha and probably to the tree root system. Cation uptake by fungi is usually achieved by proton pumps, which acidify their near environment (Lian et al., 2007). Protons diffusing into the biotite substitute the potassium in the interlayer and ultimately cause the partial transformation of biotite into potassium-free vermiculite adjacent to the hypha. The role of the fungi in the oxidation of Fe(II), and especially whether this is an active biological process or a secondary effect of the fungal weathering of biotite, is unclear. Microcavities formed during the very early stages of contact may facilitate the penetration of oxidizing compounds or exudates into the biotite structure, possibly causing the Fe(II) oxidation. The formation of vermiculite and/or Fe(III) oxide subdomains is commonly reported to be the first step in biotite weathering under abiotic acidic conditions in liquid media (Murakami et al., 2003). However, here we demonstrate,

under close to natural conditions and in a liquid-free medium, that such secondary minerals can also be formed in relatively short periods at the interface between living fungal hyphae and biotite.

The mechanism documented in this study is a significant advance on previous simplistic concepts of biotic weathering relying solely on the effects of fungal exudates (i.e., organic acids, ligands, and siderophores) released into the soil pore water. Those exudates are thought to consist of aqueous ligands for elements of biological interest, for example oxalic acid, which strongly binds iron in solution, hence thermodynamically favoring the dissolution of iron-bearing minerals.

In this respect, our findings indicate that fungal weathering is predominantly occurring at the hypha-mineral interface with an early mechanical forcing acting in concert with later chemical alteration of micaceous minerals. Through weakening of the biotite lattice structure and the formation of microcavities (increase of mineral surface area), the mechanical forcing of the mineral surface by the hypha greatly enhances the chemical weathering rates, which in turn will promote further physical breakdown of the mineral. This mechanical-chemical weathering interplay at the hypha-mineral interface therefore provides the ectomycorrhizal fungus with a hitherto unsuspected means to weather rocks and to actively acquire essential nutrients for plant growth in return for photosynthate carbon. Ultimately these processes form soils. Given the ubiquitous occurrence of ectomycorrhizal fungi in symbiotic association in boreal and temperate forests, these findings have major implications for our understanding of the link between biologically induced rock weathering and the carbon cycle at the global scale.

ACKNOWLEDGMENTS

Funding from the UK Natural Environment Research Council "Weathering Science Consortium" NE/C004566/1 is acknowledged. We thank B. Yardley, M. Krom, and D. Morgan for their help during the preparation of the manuscript. We also thank J. Raabe and the staff of the PolLux beamline at the Swiss Light Source for their contribution during the scanning transmission X-ray microscopy measurements and UK-Environsync2 for travel funds for the synchrotron work.

REFERENCES CITED

Adeyemi, A.O., and Gadd, G.M., 2005, Fungal degradation of calcium-, lead- and silicon-bearing minerals: Biometals, v. 18, p. 269–281, doi: 10.1007/s10534-005-1539-2.

Balogh-Brunstad, Z., Keller, C.K., Gill, R.A., Bormann, B.T., and Li, C.Y., 2008, The effect of bacteria and fungi on chemical weathering and chemical denudation fluxes in pine growth experiments: Biogeochemistry, v. 88, p. 153–167, doi: 10.1007/s10533-008-9202-y.

Banfield, J.F., and Nealson, K.H., eds., 1997, Geomicrobiology: Interactions between microbes and minerals: Mineralogical Society of America Reviews in Mineralogy, v. 35, 448 p.

Bastmeyer, M., Deising, H.B., and Bechinger, C., 2002, Force exertion in fungal infection: Annual Review of Biophysics and Biomolecular Structure, v. 31, p. 321–341, doi: 10.1146/annurev.biophys.31.091701.170951.

Bechinger, C., Giebel, K.-F., Schnell, M., Leiderer, P., Deising, H.B., and Bastmeyer, M., 1999, Optical measurements of invasive forces exerted by appressoria of a plant pathogenic fungus: Science, v. 285, p. 1896–1899, doi: 10.1126/science.285.5435.1896.

Beerling, D.J., and Berner, R.A., 2005, Feedbacks and the coevolution of plants and atmospheric CO2: National Academy of Sciences Proceedings, v. 102, p. 1302–1305, doi: 10.1073/pnas.0408724102.

Berner, R.A., 2004, A model for calcium, magnesium and sulfate in seawater over Phanerozoic time: American Journal of Science, v. 304, p. 438–453, doi: 10.2475/ajs.304.5.438.

Derry, L.A., 2006, Fungi, weathering, and the emergence of animals: Science, v. 311, p. 1386–1387, doi: 10.1126/science.1124183.

Ek, H., 1997, The influence of nitrogen fertilization on the carbon economy of Paxillus involutus in ectomycorrhizal association with Betula pendula: New Phytologist, v. 135, p. 133–142, doi: 10.1046/j.1469-8137.1997.00621.x.

Gadd, G.M., 2007, Geomycology: Biogeochemical transformations of rocks, minerals, metals and radionuclides by fungi, bioweathering and bioremediation: Mycological Research, v. 111, p. 3–49, doi: 10.1016/j.mycres.2006.12.001.

Harold, F.M., 2002, Force and compliance: Rethinking morphogenesis in walled cells: Fungal Genetics and Biology, v. 37, p. 271–282, doi: 10.1016/S1087-1845(02)00528-5.

Heckman, D.S., Geiser, D.M., Eidell, B.R., Stauffer, R.L., Kardos, N.L., and Hedges, S.B., 2001, Molecular evidence for the early colonization of land by fungi and plants: Science, v. 293, p. 1129–1133, doi: 10.1126/science.1061457

Högberg, M.N., and Högberg, P., 2002, Extramatrical ectomycorrhizal mycelium contributes one-third of microbial biomass and produces, together with associated roots, half the dissolved organic carbon in a forest soil: New Phytologist, v. 154, p. 791–795, doi: 10.1046/j.1469-8137.2002.00417.x.

Jongmans, A.G., van Breemen, N., Lundstrom, U., van Hees, P.A.W., Finlay, R.D., Srinivasan, M., Unestam, T., Giesler, R., Melkerud, P.A., and Olsson, M., 1997, Rock-eating fungi: Nature, v. 389, p. 682–683, doi: 10.1038/39493.

Kennedy, M., Droser, M., Mayer, L.M., Pevear, D., and Mrofka, D., 2006, Late Precambrian oxygenation: Inception of the clay mineral factory: Science, v. 311, p. 1446–1449, doi: 10.1126/science.1118929.

Kraemer, S.M., 2004, Iron oxide dissolution and solubility in the presence of siderophores: Aquatic Sciences, v. 66, p. 3–18, doi: 0.1007/s00027–003–0690–5.

Lian, B., Wang, B., Pan, M., Liu, C., and Teng, H.H., 2007, Microbial release of potassium from K-bearing minerals by thermophilic fungus *Aspergillus fumigatus*: Geochimica et Cosmochimica Acta, v. 72, p. 87–98, doi: 10.1016/j.gca.2007.10.005.

Money, P.N., 1999, Fungus punches its way in: Science, v. 201, p. 332–333.

Moulton, K.L., West, J., and Berner, R.A., 2000, Solute flux and mineral mass balance approaches to the quantification of plant effects on silicate weathering: American Journal of Science, v. 300, p. 539–570, doi: 10.2475/ajs.300.7.539.

Murakami, T., Utsunomiya, S., Yokoyama, T., and Kasama, T., 2003, Biotite dissolution processes and mechanisms in the laboratory and in nature: Early stage weathering environment and vermiculitization: American Mineralogist, v. 88, p. 377–386.

Noe, D.C., LaVan, D.A., and Veblen, D., 1999, Lap shear testing of biotite and phlogopite crystals and the application of interferometric strain/displacement gages to mineralogy: Journal of Geophysical Research, v. 104, p. 17,811–17,822, doi: 10.1029/1999JB900074.

Read, D.J., and Perez-Moreno, J., 2003, Mycorrhizas and nutrient cycling in ecosystems—A journey towards relevance?: New Phytologist, v. 157, p. 475–492, doi: 10.1046/j.1469-8137.2003.00704.x.

Remy, W., Taylor, T.N., Hass, H., and Kerp, H., 1994, Four hundred-million-year-old vesicular arbuscular mycorrhizae: National Academy of Sciences Proceedings, v. 91, p. 11841–11843, doi: 10.1073/pnas.91.25.11841.

Wallander, H., and Wickman, T., 1999, Biotite and microcline as potassium sources in ectomycorrhizal and non-mycorrhizal Pinus sylvestris seedlings: Mycorrhiza, v. 9, p. 25–32, doi: 10.1007/s005720050259.

Wierzchos, J., and Ascaso, C., 1998, Mineralogical transformation of bioweathered granitic biotite, studied by HRTEM: Evidence for a new pathway in lichen activity: Clays and Clay Minerals, v. 46, p. 446–452, doi: 10.1346/CCMN.1998.0460409.

Wosten, H.A.B., De Vries, O.M.H., and Wessels, J.G.H., 1993, Interfacial self-assembly of a fungal hydrophobin into a hydrophobic rodlet layer: The Plant Cell, v. 5, p. 1567–1574, doi: 10.2307/3869739.

Manuscript received 24 November 2008
Revised manuscript received 13 February
Manuscript accepted 19 February 2009

Printed in USA